EDGE ARTICLE

Check for updates

Synthesis of Ni II porphyrin—Ni II 5,15-diazaporphyrin hybrid tapes†

Lina Wang,[a] Zian Liao,[a] Peng Lin,[a] Yingying Jia,[a] Le Liu,[a] Ling Xu,[a] Mingbo Zhou,[a] Bangshao Yin,[a] Yutao Rao,[a] Akito Nakai,[b] Takayuki Tanaka,[b] Daiki Shimizu,[b] Atsuhiro Osuka[a] and Jianxin Song [ID] *[a]

Ni II porphyrin (P) and Ni II 5,15-diazaporphyrin (DAP) hybrid tapes were synthesized by Suzuki–Miyaura cross-coupling reactions of *meso*- or β-borylated P with β-brominated DAP followed by intramolecular oxidative fusion reactions. *Meso*-β doubly linked hybrid tapes were synthesized by oxidation of singly linked precursors with DDQ-FeCl$_3$. Synthesis of triply linked hybrid tapes was achieved by oxidation with DDQ-FeCl$_3$-AgOTf with suppression of peripheral β-chlorination. In these tapes, DAP segments were present as a 20π-electronic unit, but their local antiaromatic contribution was trivial. Remarkably, these hybrid tapes were stable and exhibited extremely enhanced absorption bands in the NIR region and multiple reversible redox waves. A pentameric hybrid tape showed a remarkably sharp and red-shifted band at 1168 nm with $\varepsilon = 5.75 \times 10^5$ M^{-1} cm^{-1}. Singly linked P-DAP dyads were oxidized with DDQ-FeCl$_3$ to give stable radicals, which were oxidized further to afford dimeric hybrid tapes possessing a nitrogen atom at the peripheral-side *meso*-position.

Introduction

Highly conjugated molecules have attracted considerable interest in light of their applications in diverse materials chemistry.[1] As representative molecules, *meso–meso*, β-β, β-β triply linked Zn II-porphyrin tapes were developed by oxidative conversion of *meso–meso* singly linked Zn II-porphyrin oligomers.[2,3] This conversion caused an orthogonal-to-coplanar structural change to realize remarkable red-shifts of absorption, which eventually reached the infrared region.[2] While a range of potential applications of porphyrin tapes have been demonstrated,[3] they became increasingly unstable upon elongation of the array owing to the steady lift-up of the HOMO level, which is a serious drawback.[2a] We hypothesized that nitrogen doping at the *meso*-positions of a porphyrin tape may stabilize the HOMO and induce novel optical and electronic properties.[4] Furthermore, nitrogen-doped porphyrin tapes could be appealing as a unique and discrete N-doped graphene model.[5] 5,15-Diazaporphyrins have been explored by Matano *et al.* and

Shinokubo *et al.*,[4,6–8] but porphyrin-diazaporphyrin hybrid tapes have not been reported before.
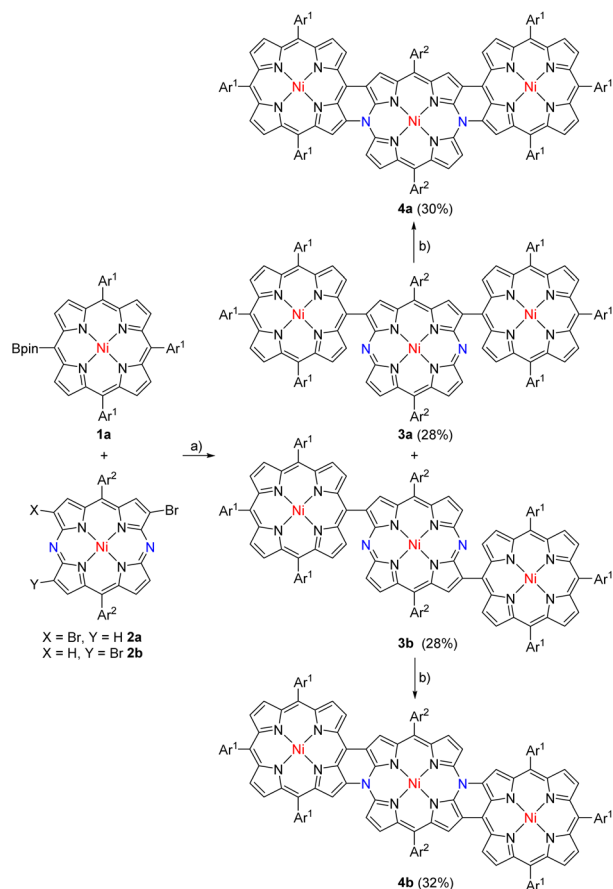
Results and discussion

In this paper, we report the synthesis of nitrogen-doped porphyrin tapes consisting of Ni II-porphyrin (P) and Ni II-5,15-diazaporphyrin (DAP). Synthetic routes were concise, involving Suzuki–Miyaura coupling and a subsequent intramolecular oxidative fusion reaction. As the first trial, isomeric triads **3a** and **3b** were prepared in 28% yields, respectively, by the cross-coupling reactions of **1a** with **2** (*ca.* 1 : 1 mixture of **2a** and **2b**) followed by chromatographic separation (Scheme 1). Triads **3a** and **3b** were been to be *syn-* and *anti-*isomers, respectively, by X-ray analysis (Fig. 1). In both triads, the DAP segment showed a planar structure but P segments showed less planar structures. The dihedral angles between DAP and P were 74.6° and 53.8° in **3a** and 65.3° in **3b**, respectively.

We attempted the synthesis of *meso*, β doubly linked porphyrin tapes from **3a** and **3b**. Through many attempts, we found that hybrid tapes **4a** and **4b** were obtained in 30% and 32% yields by oxidation of **3a** and **3b**, respectively, with DDQ and FeCl$_3$ (Scheme 1). Hybrid tapes **4a** and **4b** showed parent-ion peaks at $m/z = 2459.1427$ (calcd for [C$_{160}$H$_{168}$N$_{14}$Ni$_3$]$^+$ = 2459.1631) and at $m/z = 2459.1584$ (calcd for [C$_{160}$H$_{168}$N$_{14}$Ni$_3$]$^+$ = 2459.1631), respectively. X-ray diffraction revealed the *anti*-structure of **4b** to be considerably bent (Fig. 1). Importantly, **4b** had a neutral 20π-DAP unit with average N$_{meso}$–C$_\alpha$, N$_{meso}$–C$_\beta$, and C$_{meso}$–C$'_\beta$ bond lengths of 1.38, 1.41, and 1.44 Å, respectively,

[a]Key Laboratory of Chemical Biology and Traditional Chinese Medicine Research (Ministry of Education of China), Key Laboratory of the Assembly and Application of Organic Functional Molecules of Hunan Province, College of Chemistry and Chemical Engineering, Hunan Normal University, Changsha 410081, China. E-mail: jxsong@hunnu.edu.cn

[b]Department of Chemistry, Graduate School of Science, Kyoto University, Sakyo-ku, Kyoto 606-8502, Japan

Scheme 1 Synthesis of **4a** and **4b**. Reagents and conditions: (a) Pd$_2$(dba)$_3$, PPh$_3$, Cs$_2$CO$_3$, CsF, toluene/DMF, reflux, 48 h; (b) DDQ-FeCl$_3$, CH$_2$Cl$_2$/MeNO$_2$, r.t., 1 h. Ar^1 = 3,5-di-*tert*-butylphenyl, Ar^2 = 2,4,6-trimethylphenyl.
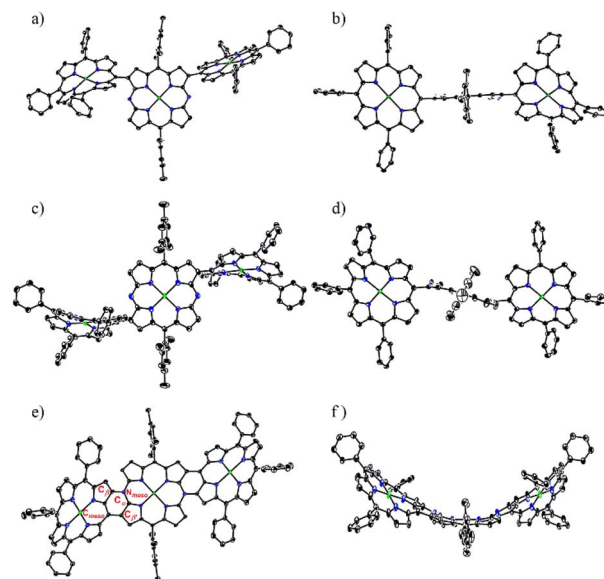

Fig. 1 X-ray crystal structures of **3a**, **3b** and **4b**. (a) Top view and (b) side view of **3a**. (c) Top view and (d) side view of **3b**. (e) Top view and (f) side view for one configuration of **4b**. Top view and side view refers to the central DAP unit. Solvent molecules, *tert*-butyl of *meso*-aryl substituents, and all hydrogen atoms have been omitted for clarity. The thermal ellipsoids of **3a** are scaled to 20% probability. The thermal ellipsoids of **3b** are scaled to 50% probability. The thermal ellipsoids of **4b** are scaled to 30% probability.
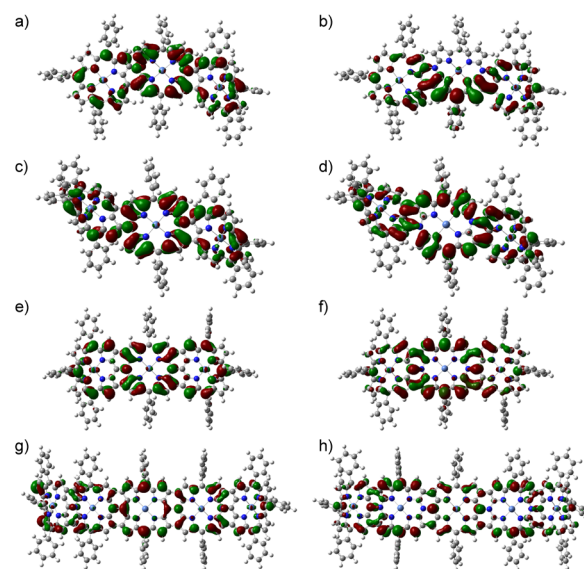

Fig. 2 Molecular orbital diagrams of **4a**, **4b**, **6** and **10**. (a) HOMO and (b) LUMO of **4a**. (c) HOMO and (d) LUMO of **4b**. (e) HOMO and (f) LUMO of **6**. (g) HOMO and (h) LUMO+1 of **10**. Molecular orbital diagrams are based on optimized structures, 3,5-di-*tert*-butylphenyl and 2,4,6-trimethylphenyl have been replaced by phenyl for simplification. DFT calculations were performed at the B3LYP/6-31G(d) level.

embedded in a bent-tape structure. Observed N$_{meso}$–C$_\alpha$ and N$_{meso}$–C$_\beta$ bond distances were distinctly shorter than the normal N–C bond length (1.47 Å). In line with the structures, a singlet set and two sets of signals due to Ar^2 protons were observed for **4b** and **4a**, respectively. In addition, singlet signals due to the β proton at the DAP unit were observed at 9.04 and 9.01 ppm in **4a** and **4b**, respectively. These high chemical shifts were contrary to what was expected for a paratropic ring current arising from the 20π-DAP unit judging from low chemical shifts (4.6–3.3 ppm) of antiaromatic 20π-DAP monomers.[4,8] Instead, DFT calculations indicated that the molecular orbitals of **4a** and **4b** were well spread over entire tapes (Fig. 2a–d), and the local antiaromaticity of DAP units did not remain in **4a** or **4b** based on NICS(0) values therein (Fig. S6, S2†).

Triply linked hybrid tape **6** was synthesized *via* triads **5a** and **5b**, which were prepared in 33% and 37% yields, respectively, by the cross-coupling reactions of **1b** with **2** followed by chromatographic separation (Scheme 2). *Syn*- and *anti*-structures were confirmed for **5a** and **5b**, respectively, by X-ray analysis (Fig. 3). In both cases, the DAP segment showed a planar structure, and P units showed less planar structures. The dihedral angles between DAP and P were 45.1° and 45.2° in **5a** and 25.7° in **5b**, respectively.

In the next step, oxidation of a mixture of **5a** and **5b** with DDQ and FeCl$_3$ under similar conditions led to the formation of **6** (25%) along with β-chlorinated hybrid tapes **6-Cl** (10%) (Scheme 2). Meanwhile, we found that addition of an excess
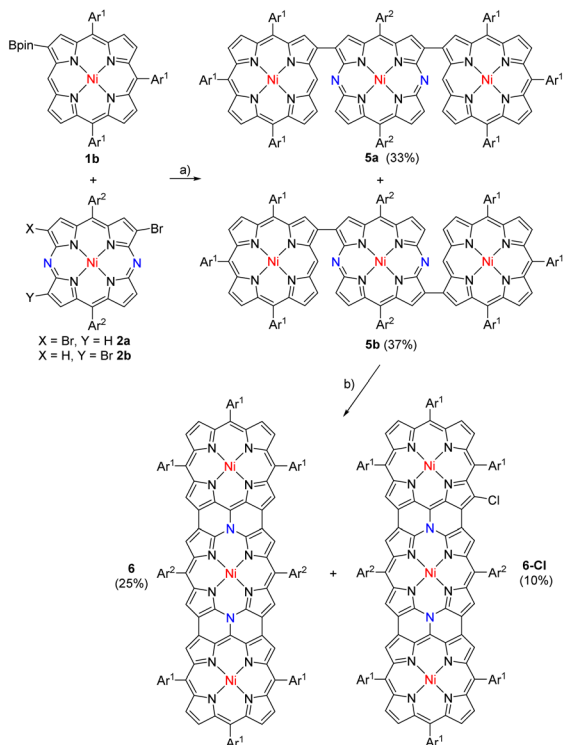
Scheme 2 Synthesis of **6**. Reagents and conditions: (a) Pd$_2$(dba)$_3$, PPh$_3$, Cs$_2$CO$_3$, CsF, toluene/DMF, reflux, 48 h; (b) DDQ–FeCl$_3$–AgOTf, CH$_2$Cl$_2$/MeNO$_2$, r.t., 1 h. Ar^1 = 3,5-di-*tert*-butylphenyl, Ar^2 = 2,4,6-trimethylphenyl.
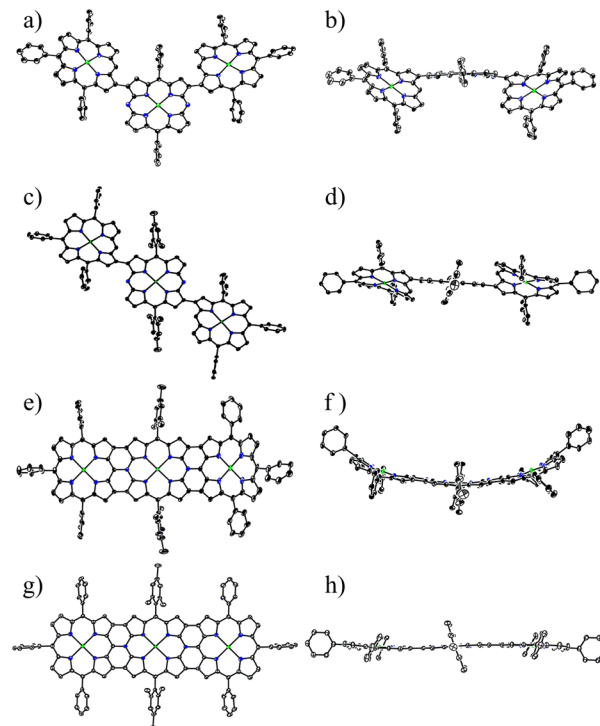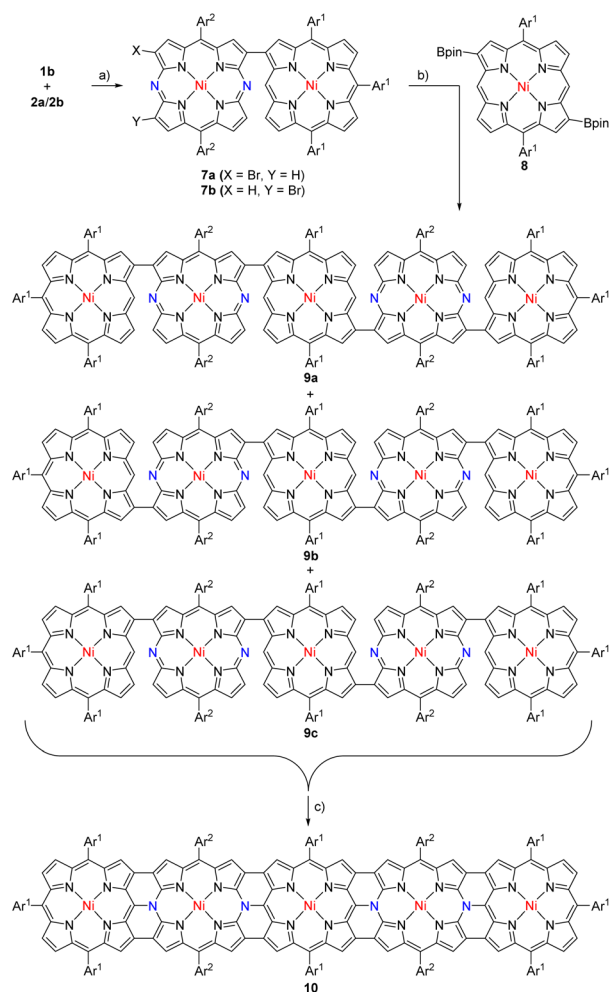

Fig. 3 X-ray crystal structures of **5a**, **5b** and **6**. (a) Top view and (b) side view of **5a**. (c) Top view and (d) side view of **5b**. (e) Top view and (f) side view of **6**. (g) Top view and (h) side view for another configuration of **6**. Solvent molecules, *tert*-butyl of *meso*-aryl substituents, and all hydrogen atoms have been omitted for clarity. The thermal ellipsoids of **5a** and **5b** are scaled to 50% probability. The thermal ellipsoids of **6** are scaled to 30% probability.

amount of AgOTf could improve the yield of **6** by suppressing the formation of β-chlorinated tapes. Namely, a solution of **5a** and/or **5b** in CH$_2$Cl$_2$ was stirred at room temperature for 1 h in the presence of DDQ (10 equiv.), FeCl$_3$ (10 equiv.), and AgOTf (100 equiv.), and subsequent chromatographic separation gave **6** in 45% yield. The parent-ion peak of **6** was detected at m/z = 2455.1405 (calcd for [C$_{160}$H$_{164}$N$_{14}$Ni$_3$]$^+$ = 2455.1318 ([M]$^+$)). The structure of **6** was confirmed by X-ray diffraction. In the crystal of **6**, two structures were found: a bent structure (Fig. 3e and f) and planar structure (Fig. 3g and h). Here, the center was a formal 20π-DAP carrying two neutral *meso*-nitrogen atoms with average N$_{meso}$–C$_\alpha$, N$_{meso}$–C$_{meso}$, and C$_\beta$–C$_\beta$ bond lengths of 1.381, 1.425, and 1.428 Å, and of 1.373, 1.417, and 1.410 Å, respectively. The ^{1}H NMR spectrum indicated one pair of doublets due to edge β-protons at 8.81 and 8.76 ppm and two singlet signals due to inner β-protons at 9.14 and 8.13 ppm being much lower as compared with the trimeric Zn^{II} porphyrin tape.[9] These data also excluded a possible paratropic ring current of 20π-DAP. DFT calculations indicated that the molecular orbital of **6** was well delocalized over the whole tape (Fig. 2e and f).

We also attempted the synthesis of a pentameric hybrid tape **10** (Scheme 3). Brominated dyad **7** (*ca.* 1 : 1 mixture of **7a** and **7b**) was prepared by the cross-coupling reaction of **1b** with **2** in 51% yield. This brominated mixture was coupled with diborylated Ni^{II} porphyrin **8** to afford a mixture of pentameric precursors (**9a**, **9b**, and **9c**) in 61% yield. The parent-ion peak was detected

at m/z = 3804.6985 (calcd for (C$_{244}$H$_{249}$N$_{24}$Ni$_5$)$^+$ = 3804.6984 ([M + H]$^+$)). Oxidation of pentameric precursors with DDQ, FeCl$_3$, and AgOTf produced pentameric hybrid tape **10** in 16% yield. The parent-ion peak of **10** was detected at m/z = 3791.5733 (calcd for [C$_{244}$H$_{236}$N$_{24}$Ni$_5$]$^+$ = 3791.5955 ([M]$^+$)). The ^{1}H NMR spectrum showed one pair of doublets at 8.82 and 8.76 ppm and four singlets at 9.17, 9.05, 8.20, and 8.00 ppm. These data indicated the trivial contribution of a paratropic ring current of 20π-DAP but a global diatropic ring current. DFT calculations indicated a delocalized nature of HOMO and LUMO+1 over the entire tape (Fig. 2g and h).
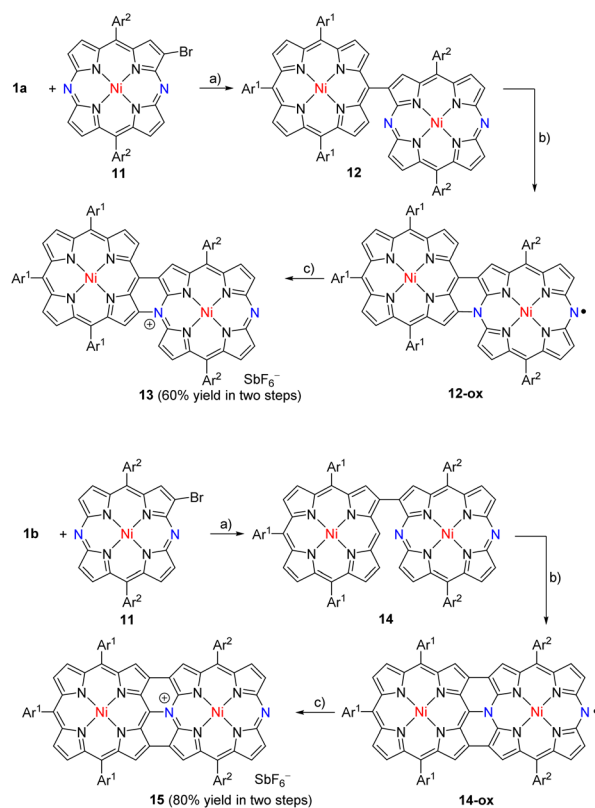
Finally, we examined the synthesis of dimeric hybrid tapes which had *N*-unsubstituted DAP at the periphery. Meso-β linked P—DAP dyad **12** was prepared by the cross-coupling of **1a** (ref. 10) with **11** (ref. 11) in 71% yield (Scheme 4). Oxidation of **12** with DDQ and FeCl$_3$ in a mixture of CH$_2$Cl$_2$ and nitromethane at room temperature for 1 h gave a stable product, **12-ox**, which exhibited the parent-ion peak at 1531.6771 (calcd for C$_{98}$H$_{99}$N$_{10}$Ni$_2$, m/z = 1531.6756 ([M]$^+$)), which was 2H less than that of **12**. The ^{1}H NMR spectrum of **12-ox** was extremely broad, suggesting its radical character. In fact, **12-ox** in degassed toluene exhibited an EPR signal at g = 1.9995 (Fig. S1–S23†). The signal did not have hyperfine coupling (hfc) features, indicating small hfc constants due to effective spin delocalization over the π-system. It is important to note that **12-ox** is
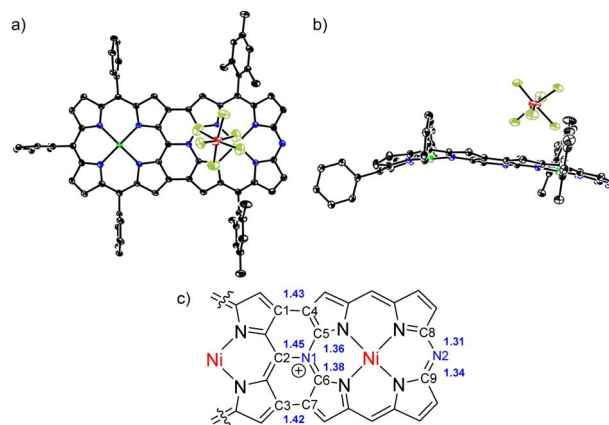
Scheme 3 Synthesis of **10**. Reagents and conditions: (a) Pd$_2$(dba)$_3$, PPh$_3$, Cs$_2$CO$_3$, CsF, toluene/DMF, reflux, 24 h; (b) Pd$_2$(dba)$_3$, PPh$_3$, Cs$_2$CO$_3$, CsF, toluene/DMF, reflux, 48 h; (c) DDQ–FeCl$_3$–AgOTf, CH$_2$Cl$_2$/MeNO$_2$, r.t., 1 h. Ar^1 = 3,5-di-*tert*-butylphenyl, Ar^2 = 2,4,6-trimethylphenyl.

Scheme 4 Synthesis of **13** and **15**. Reagents and conditions: (a) Pd$_2$(dba)$_3$, PPh$_3$, Cs$_2$CO$_3$, CsF, toluene/DMF, reflux, 48 h; (b) DDQ, FeCl$_3$, CH$_2$Cl$_2$/MeNO$_2$, r.t., 1 h; (c) TBPA·SbF$_6$, CH$_2$Cl$_2$, r.t., 1 h. Ar^1 = 3,5-di-*tert*-butylphenyl, Ar^2 = 2,4,6-trimethylphenyl.

was observed at m/z = 1531.6747 (calcd for C$_{98}$H$_{99}$N$_{10}$Ni$_2$, m/z = 1531.6756 ([M-SbF$_6$]$^+$)). The ^{1}H NMR spectrum of **15** exhibited broad (but characteristically high-field-shifted) signals at 6.74 and 6.70 ppm due to the β-protons at the *meso*-nitrogen side. The structure of **15** was confirmed by X-ray analysis to be a triply linked P—DAP hybrid bearing a SbF$_6^-$ counter anion (Fig. 4). In

stable under ambient conditions. Further oxidation of **12-ox** with tris(4-bromophenyl)aminium hexafluoroantimonate gave the SbF$_6^-$ salt **13** in 60% yield in two steps. The fused dimer **13** showed the parent-ion peak at 1531.6747 (calcd for C$_{98}$H$_{99}$N$_{10}$Ni$_2$, m/z = 1531.6756 ([M-SbF$_6$]$^+$)). Different from the trimeric and pentameric hybrid tapes, the DAP unit had an 18π-electronic system. The ^{1}H NMR spectrum of **13** showed peaks in the low-field region due to the diamagnetic current. On the basis of these data, we thought that **12-ox** was a neutral radical (Scheme 4), but we failed to obtain its single crystals.

Similarly, β-β linked P—DAP dyad **14** was prepared by the cross-coupling of **1b** with **11** in 75% yield. It was oxidized with DDQ and FeCl$_3$ to yield **14-ox** as an intermediate, which exhibited the parent-ion peak at 1532.6794 (calcd for C$_{98}$H$_{100}$N$_{10}$Ni$_2$, m/z = 1532.6834 ([M + H]$^+$)), which was 2H less than that of **14**. Radical **14-ox** in toluene showed an EPR signal similar to **12-ox** at g = 1.9985 without hfc splitting. Radical **14-ox** was also stable. Further oxidation of **14-ox** with TBPA·SbF$_6$ gave hybrid tape **15** in a two-step yield of 80%. The parent-ion peak

Fig. 4 X-ray crystal structure of **15**. (a) Top view, (b) side view and (c) selected bond lengths of **15**. Solvent molecules, *tert*-butyl of *meso*-aryl substituents, and all hydrogen atoms have been omitted for clarity. The thermal ellipsoids are scaled to 30% probability.
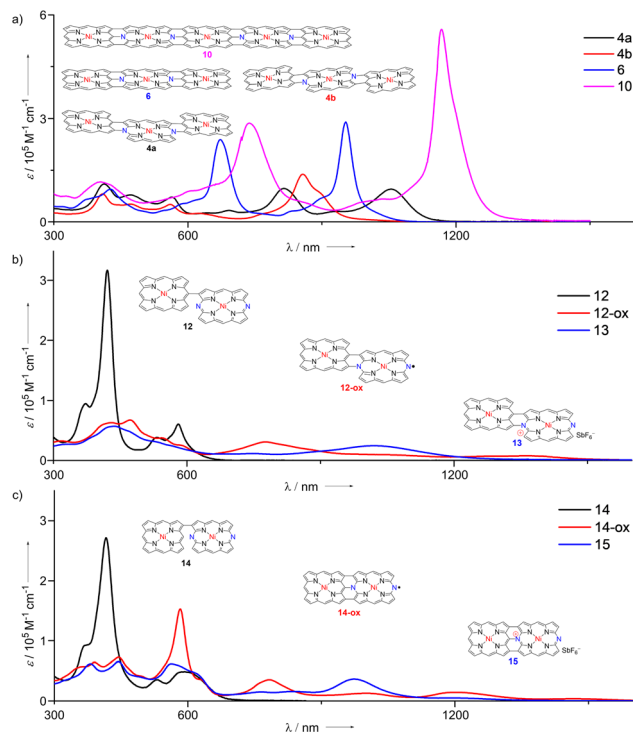
Fig. 5 UV/Vis absorption spectra of **4a**, **4b**, **6**, **10**, **12**, **12-ox**, **13**, **14**, **14-ox**, and **15**. (a) UV/Vis absorption spectra of **4a**, **4b**, **6**, and **10**. (b) UV/Vis absorption spectra of **12**, **12-ox**, and **13**. (c) UV/Vis absorption spectra of **14**, **14-ox**, and **15**.

15, the P moiety took a domed form but the DAP moiety was almost planar. The bond lengths of C(1)–C(4), C(2)–N(1) and C(3)–C(7) bonds were 1.432(8), 1.449(7), and 1.422(8) Å, respectively. Importantly, the bond lengths of C(5)–N(1) (1.360(7) Å) and C(6)–N(1) bonds (1.375(7) Å) were distinctly shorter than the C(2)–N(1) bond, revealing conjugation in the DAP unit through a positively charged quaternary nitrogen atom.

Fig. 5a shows the UV/Vis absorption spectra of **4a**, **4b**, **6**, and **10** in CH_2Cl_2. The absorption spectra of **4a** and **4b** are different, showing absorption bands at 412, 473, 565, 814, and 1054 nm and at 409, 473, 560, 624, and 857 nm, respectively, which reflected different *syn*- and *anti*-molecular structures. Curiously, the spectral features of **4a** and **4b** were quite different from those of corresponding Zn^{II} porphyrin tapes.[12] The observed

red-shifted band at 1054 nm for **4a** was remarkable because the anti-isomer of the *meso*-β doubly linked Zn^{II} porphyrin tape showed an intensified band as compared with the syn-isomer.[13] Triply-linked hybrid tape **6** displayed three major absorption bands at 427, 672, and 953 nm. The molar extinction coefficient of the Q band ($\lambda = 953$ nm) was 2.90×10^5 M^{-1} cm^{-1}, which is significantly larger than that of the original Zn^{II} porphyrin trimer tape ($\lambda_{max} = 1406$ nm, $\varepsilon = 1.48 \times 10^5$ M^{-1} cm^{-1}).[9] It is interesting to note that **4a** showed a more red-shifted absorption band than that of **6**.

Dimeric tape **13** displayed a very broad absorption spectrum with weak peaks at 436, 748, and 1020 nm (Fig. 5b). **12-ox** showed a very broad absorption spectrum with weak peaks at 316, 430, 472, 543, 776, and 1357 nm, which are characteristic of porphyrinoid radical species.[13] **15** displayed a broad absorption spectrum with peaks at 381, 444, 563, 766, 834, and 974 nm (Fig. 5c). Similarly, the absorption spectrum of **14-ox** shows bands at 390, 444, 583, 783, 1000, and 1200 nm with a low tail reaching to *ca.* 1600 nm.

Electrochemical properties were examined by cyclic voltammetry and differential pulse voltammetry (Table 1). Dimer **14** exhibited an irreversible first oxidation potential at 0.53 V and a reversible first reduction potential at −1.26 V, which corresponded to that of **Ni-Por** (0.58 V) and that of **Ni-DAP** (−1.32 V), respectively. These results revealed that first oxidation would occur at the porphyrin site, and first reduction would occur at the DAP site. Radical **14-ox** showed reversible redox waves at −0.24, 0.80, and −0.59 V, and **12-ox** displayed reversible redox waves at −0.32, 0.74, and −0.68 V. Fairly reversible redox waves and a narrow HOMO–LUMO gap of **14-ox** (0.35 eV) and **12-ox** (0.36 eV) are characteristics of porphyrinoid radicals.[14] The first reduction and oxidation potentials of cation species **15** (−0.22 and 0.80 V) should correspond to the first and second oxidation potentials of radical **14-ox** (−0.24 and 0.80 V), and this observation could also be found between **12-ox** and **13**.[15]

As a rare case, doubly linked hybrid tapes **4a** and **4b** showed eight reversible waves at 1.03, 0.89, 0.71, 0.20, −0.24, −1.40, −1.78, and −1.98 V, and at 1.30, 0.75, 0.63, 0.19, −0.23, −1.54, −1.63, and −2.06 V, respectively, suggesting their potential as electron reservoirs. Trimeric hybrid tape **6** showed nine reversible waves at 1.20, 0.86, 0.75, 0.25, −0.16, −1.36, −1.58, −1.99, and −2.24 V. Pentameric hybrid tape **10** displayed weak reversible waves at 0.62, probably due to its poor solubility. The electrochemical HOMO–LUMO gaps increased in the order of

Table 1 Electrochemical properties of **4a**, **4b**, **6**, **10**, **13** and **15** in benzonitrile with 0.1 M *n*-Bu$_4$NPF$_6$[a]

Cpd.	$E_{ox.5}$ (V)	$E_{ox.4}$ (V)	$E_{ox.3}$ (V)	$E_{ox.2}$ (V)	$E_{ox.1}$ (V)	$E_{red.1}$ (V)	$E_{red.2}$ (V)	$E_{red.3}$ (V)	ΔE_{HL}[c] (eV)
4a	1.03	0.89	0.71	0.20	−0.24	−1.40	−1.78	−1.98	1.16
4b	1.30[b]	0.75	0.63	0.19	−0.23	−1.54	−1.63	−2.06	1.31
6	1.20	0.86	0.75	0.25	−0.16	−1.36	−1.58	−1.99	1.20
10				1.00	0.62	−0.42	−2.26	−2.42	1.04
13					0.75	−0.28	−0.67		1.03
15					0.80	−0.24	−0.57		1.04

[a] Potentials [V] *vs.* ferrocene/ferrocenium ion. Scan rate = 0.05 V s^{-1}; glassy carbon working electrode and Pt wire counter electrode; supporting electrolyte = 0.1 M *n*Bu$_4$NPF$_6$ in benzonitrile; Ag/AgNO$_3$ reference electrode. [b] Irreversible peaks. [c] Electrochemical HOMO–LUMO gaps ($\Delta E_{HL} = e (E_{ox.1} - E_{red.1})$ [eV]).

10 (1.04 eV) < **4a** (1.16 eV) < **6** (1.20 eV) < **4b** (1.31 eV), which was in agreement with their optical properties. The cationic tapes **13** and **15** showed small HOMO–LUMO gaps, which were comparable with that of **10**.

Conclusions

In summary, we have developed a concise protocol to synthesize P–DAP hybrid tapes by Suzuki–Miyaura cross-coupling reactions and subsequent suitable oxidations. In hybrid tapes with DAP, the DAP units were 20π-electronic systems, but their local antiaromatic effects were quite minor. Dimeric tapes were synthesized as cationic species carrying an 18π-electronic DAP unit. These hybrid tapes were stable and exhibited intriguing properties, such as nine reversible redox waves for **6** and extremely enhanced Q-like absorption bands at 1168 nm with $\varepsilon = 5.75 \times 10^5$ M^{-1} cm^{-1} for **10**. Exploration of more extended porphyrin–DAP hybrid nanotapes is underway in our laboratory.

Data availability

All experimental data and detailed experimental procedures, are available in the ESI.†

Author contributions

J. Song designed and conducted the project. L. Wang, Z. Liao, P. Lin, and Y. Jia performed the synthesis and characterization, and measured optical and electrochemical properties. L. Xu, and Y. Rao performed X-ray diffraction. A. Nakai, T. Tanaka, and D. Shimizu performed EPR experiments and analysis. L. Xu, Y. Rao, and T. Tanaka performed DFT calculations. L. Xu, M. Zhou, B. Yin, A. Nakai, Y. Rao, T. Tanaka, J. Song, and A. Osuka prepared the manuscript.

Conflicts of interest

There are no conflicts of interest to declare.

Acknowledgements

Notes and references

1 (a) M. Stępień, E. Gońka, M. Żyła and N. Sprutta, *Chem. Rev.*, 2017, **117**, 3479; (b) A. Borissov, Y. K. Maurya, L. Moshniaha, W.-S. Wong, M. Żyła-Karwowska and M. Stępień, *Chem. Rev.*, 2022, **122**, 565.

2 (a) A. Osuka and A. Tsuda, *Science*, 2001, **293**, 79; (b) D. Kim and A. Osuka, *J. Phys. Chem.*, 2003, **107**, 8791; (c) D. Kim and A. Osuka, *Acc. Chem. Res.*, 2004, **37**, 735.

3 (a) Y. Nakamura, N. Aratani, H. Shinokubo, A. Takagi, T. Kawai, T. Matsumoto, Z. S. Yoon, D. Y. Kim, T. K. Ahn, D. Kim, A. Muranaka, N. Kobayashi and A. Osuka, *J. Am. Chem. Soc.*, 2006, **128**, 4119; (b) H. Mori, T. Tanaka and A. Osuka, *J. Mater. Chem.*, 2013, **1**, 2500; (c) T. Tanaka and A. Osuka, *Chem.–Eur. J.*, 2018, **24**, 17188; (d) D. Bonifazi, M. Scholl, F. Song, L. Echegoyen, G. Accorsi, N. Armaroli and F. Diederich, *Angew. Chem., Int. Ed.*, 2003, **42**, 4966; (e) D. Bonifazi, H. Spillamn, A. Kiebele, M. de Wild, P. Seiler, F. Cheng, H.-J. Güntherodt, T. Jung and F. Diederich, *Angew. Chem., Int. Ed.*, 2004, **43**, 4759; (f) T. Sakurai, K. Shi, H. Sato, K. Tashiro, A. Osuka, A. Saeki, S. Seki, S. Tagawa, S. Sasaki, H. Masunaga, K. Osaka, M. Takata and T. Aida, *J. Am. Chem. Soc.*, 2008, **130**, 13812; (g) J.-R. Deng, M. T. González, H. Zhu, H. L. Anderson and E. Leary, *J. Am. Chem. Soc.*, 2024, **146**, 3651; (h) Z. Chen, J.-R. Deng, S. Hou, X. Bian, J. L. Swett, Q. Wu, J. Baugh, L. Bogani, G. A. D. Briggs, J. A. Mol, C. J. Lambert, H. L. Anderson and J. O. Thomas, *J. Am. Chem. Soc.*, 2023, **145**, 15265; (i) V. V. Diev, K. Hanson, J. D. Zimmerman, S. R. Forrest and M. E. Thompson, *Angew. Chem., Int. Ed.*, 2010, **49**, 5523; (j) T. Sakurai, K. Tashiro, Y. Honsho, A. Saeki, S. Seki, A. Osuka, A. Muranaka, M. Uchiyama, J. Kim, S. Ha, K. Kato, M. Takata and T. Aida, *J. Am. Chem. Soc.*, 2011, **133**, 6537.

4 Y. Matano, *Chem. Rev.*, 2017, **117**, 3138.

5 (a) X.-Y. Wang, M. Richter, Y. He, J. Björk, A. Riss, R. Rajesh, M. Garnica, F. Hennersdorf, J. J. Weigand, A. Narita, R. Berger, X. Feng, W. Auwärter, J. V. Barth, C.-A. Palma and K. Müllen, *Nat. Commun.*, 2017, **8**, 1948; (b) U. Hahn, E. Maisonhaute and J.-F. Nierengarten, *Angew. Chem., Int. Ed.*, 2018, **57**, 10635; (c) X. Guo, Z. Yuan, Y. Zhu, Z. Li, R. Huang, Z. Xia, W. Zhang, Y. Li and J. Wang, *Angew. Chem., Int. Ed.*, 2019, **58**, 16966.

6 (a) Y. Matano, T. Shibano, H. Nakano and H. Imahori, *Chem.–Eur. J.*, 2012, **18**, 6208; (b) Y. Matano, T. Shibano, H. Nakano, Y. Kimura and H. Imahori, *Inorg. Chem.*, 2012, **51**, 12879.

7 (a) Y. Matano, D. Fujii, T. Shibano, K. Furukawa, T. Higashino, H. Nakano and H. Imahori, *Chem.–Eur. J.*, 2014, **20**, 3342; (b) S. Omomo, Y. Maruyama, K. Furukawa, T. Furuyama, H. Nakano, N. Kobayashi and Y. Matano, *Chem.–Eur. J.*, 2015, **21**, 2003; (c) M. Kawamata, T. Sugai, M. Minoura, Y. Maruyama, K. Furukawa, C. Holstrom, V. N. Nemykin, H. Nakano and Y. Matano, *Chem.–Asian J.*, 2017, **12**, 816; (d) F. Abou-Chahine, D. Fujii, H. Imahori, H. Nakano, N. V. Tkachenko, Y. Matano and H. Lemmetyinen, *J. Phys. Chem. B*, 2015, **119**, 7328.

8 T. Sakurai, Y. Hiraoka, H. Tanaka, Y. Miyake, N. Fukui and H. Shinokubo, *Angew. Chem., Int. Ed.*, 2023, **62**, e202300437.

9 T. Tanaka, B. S. Lee, N. Aratani, M.-C. Yoon, D. Kim and A. Osuka, *Chem.–Eur. J.*, 2011, **17**, 14400.

10 H. Hata, H. Shinokubo and A. Osuka, *J. Am. Chem. Soc.*, 2005, **127**, 8264.

11 Y. Matano, D. Fujii, T. Shibano, K. Furukawa, T. Higashino, H. Nakano and H. Imahori, *Chem.–Eur. J.*, 2014, **20**, 3342.

12 T. Ikeda, N. Aratani, S. Easwaaramoorthi, D. Kim and A. Osuka, *Org. Lett.*, 2009, **11**, 3080.

13 (*a*) Y. Hisamune, K. Nishimura, K. Isakari, M. Ishida, S. Mori, S. Karasawa, T. Kato, S. Lee, D. Kim and H. Furuta, *Angew. Chem., Int. Ed.*, 2015, **54**, 7323; (*b*) P. Schweyen, K. Brandhorst, R. Wicht, B. Wolfram and M. Bröring, *Angew. Chem., Int. Ed.*, 2015, **54**, 8213; (*c*) Y. Tanaka, T. Yoneda, K. Furukawa, T. Koide, H. Mori, T. Tanaka, H. Shinokubo and A. Osuka, *Angew. Chem., Int. Ed.*, 2015, **54**, 10908; (*d*) T. Yoshida, W. Zhou, T. Furuyama, D. B. Leznoff and N. Kobayashi, *J. Am. Chem. Soc.*, 2015, **137**, 9258; (*e*) D. Shimizu, J. Oh, K. Furukawa, D. Kim and A. Osuka, *J. Am. Chem. Soc.*, 2015, **137**, 15584.

14 (*a*) T. Koide, K. Furukawa, H. Shinokubo, J.-Y. Shin, K. S. Kim, D. Kim and A. Osuka, *J. Am. Chem. Soc.*, 2010, **132**, 7246; (*b*) D. Shimizu, J. Oh, K. Furukawa, D. Kim and A. Osuka, *Angew. Chem., Int. Ed.*, 2015, **54**, 6613; (*c*) D. Shimizu and A. Osuka, *Chem. Sci.*, 2018, **9**, 1408.

15 (*a*) D. Shimizu, K. Fujimoto and A. Osuka, *Angew. Chem., Int. Ed.*, 2018, **57**, 9434; (*b*) K. Fujimoto, D. Shimizu and A. Osuka, *Chem.–Eur. J.*, 2019, **25**, 521.